Joachim Gröbner, Dmytro Kevorkov, Igor Chumak, Rainer Schmid−Fetzer*

Technical University of Clausthal, Institute of Metallurgy, Clausthal-Zellerfeld, Germany

Experimental investigation and thermodynamic calculation of ternary Al-Ca-Mg phase equilibria

The ternary Al−Ca−Mg phase equlibria were investigated using X-ray diffraction methods, metallography, scanning electron microscopy with energy- and wave-length-dispersive X-ray microanalysis and differential thermal analysis. The phase diagram was determined in the complete composition range. Large ternary solubilities were found for the binary phases $CaMg_2$, Al_2Ca and Al_3Ca_8. Microstructures of samples with compositions near the ternary monovariant eutectic $L \rightarrow CaMg_2 + Al_2Ca$ show remarkable rod-like crystals that are identified as intergrowth between $CaMg_2$ and Al_2Ca. A consistent thermodynamic model was developed using the Calphad method incorporating all experimental data. It was used to calculate all pertinent phase equilibria of the Al−Ca−Mg system.

Keywords: Thermodynamic modeling; Calphad; Microstructure; Phase diagram; Al−Ca−Mg

1. Introduction

Magnesium alloys are one of the most promising light-weight materials for automotive applications. The current use of Mg in automotive applications is usually limited to non-critical parts because of their restricted creep properties. Technically used alloys mainly contain Al and Zn. Rare earths additions improve creep resistance of these alloys by forming precipitates. Some attemps were made in the last decades to replace the rare earth metals by Ca. But die-sticking and hot-cracking behavior caused problems [2000Lou]. Newly developed Mg−Al−Ca-based alloys with microalloying additions of Si and Sr show significantly better tensile and compressive creep properties than the benchmark AE42 alloy [2001Luo]. This improved creep resistance is attributed to the thermal stability and the interfacial coherency of the $(Mg,Al)_2Ca$ phase in the microstructure of the alloys. [2001Pek] showed that diecasted Mg−Al−Ca alloys offer creep resistance, tensile strength and corrosion resistance comparable to commercially used Mg-alloys with rare earth additions, like AE42. These properties can be achieved with much lower costs, since the stability of these Al_2Ca precipitates is comparable to the rare earth precipitates. Improvement of tensile strength and impact toughness by Ca addition to the most commonly used AZ91 alloy is reported also by [2001Wan]. [2002Buc] described the development of new technical Mg alloys based on AZ91 with Ca and minor rare earth (Ce mischmetal), Sr and Si additions. Calcium additions for improvement of the creep properties offer several additional advantages compared to cost intensive rare earth additons. It protects the melt surface combined with less slag formation and additive loss. The Al content can be high compared to Si containing alloys, which leads to better castability. The resulting alloys show lower secondary creep rates and higher tensile strengh than AZ91combined with comparable castability and good melt handling [2002Buc]. Thin dense and compact films on Mg−Ca alloys were reported by [2001You]. These films, consisting of amorphous and microcystalline CaO/MgO oxides, improve the corrosion resistivity compared to the porous oxide films on pure Mg.

Despite the high potential of Ca additons for the technical development of Mg alloys, the phase diagram of the ternary Mg−Al−Ca system is scarcely known. A technically very important open question is the homogeneity range of the phases Al_2Ca and Mg_2Ca expected in casted alloys. During our extended study of this ternary system we found two new binary compounds in the Al−Ca system. A detailed experimental investigation and thermodynamic calculation of that binary system was already published [2001Kev1, 2001Kev2]. The purpose of this study is to present the complete Al−Ca−Mg phase diagram based on experimental work and thermodynamic modeling.

2. Experimental data in the literature

First information about the Al−Ca−Mg system was published by Portnoi and Spektorova [1948Por]. They reported a pseudobinary section Mg−Al_2Ca with a eutecitc liquid composition of about 79 at.% Mg. A ternary eutectic at about 9 at.% Al and 79 at.% Mg was also mentioned. [1959Dow] measured the eutectic temperature Mg−Al_2Ca at 535 °C and the composition between 74 and 83 at.% Mg. Their micrographs lead to the conclusion of a quasibinary eutectic composition at 78-79 at.% Mg.

A partial isothermal section of the Mg-rich corner was given by [1957Cat]. The casted alloys were annealed for 2 weeks at 450 °C, 1 month at 370 °C and 3 months at 290 °C, then quenched and examined by optical microscopy. The reported two-phase field Mg + Al_2Ca is in good agreement with the other investigations. Two three-phase equilibria were found: (Mg) + Al_2Ca + $CaMg_2$ and (Mg) + Al_2Ca + $Mg_{17}Al_{12}$ (γ). [1958Sta] separated primary phases on cooling Mg-rich alloys from the melt. A phase with composition of about 43Al, 25Ca, 32 at.% Mg was observed crystallizing in the same structure as Al_2Ca. The structure was believed to be tetragonal because of the existence of additional lines in the diffraction pattern. This "ternary compound" forms a eutectic with (Mg). [1958Sta] recognized the possibility of a solid solution of Mg in Al_2Ca instead of a separate ternary phase. Comparing to other ternary systems with similar elements like Sr, the occurrence of extended solid solution is not unlikely. For example the Al_2Sr phase dissolves 20 at.% Mg and Mg_2Sr dissolves 10 at.% Al in the Al−Mg−Sr system [1981Mak].

3. Experimental investigation

The experimental investigation of the Al−Ca−Mg phase equilibria was carried out with X-ray powder diffraction (XRD) analysis, metallographic analysis, SEM/EDX/WDX (scanning electron microscopy with both energy- and wave-length-dispersive X-ray microanalysis) and differential thermal analysis (DTA). The alloys were carefully arc melted under purified argon to avoid extensive evaporation of Mg. Starting materials were Al powder (99.8 wt.%, Alfa, Karlsruhe), Ca granules (99.5 wt.%, Alfa, Karlsruhe) and Mg pieces (99.98 wt.%, Alfa, Karlsruhe). The loss in total mass was below 3 % for all samples that went to further analysis. These as-cast alloys are rapidly quenched on the water-cooled copper mold of the arc melting furnace.

Three series of samples were prepared for XRD, these compositions are given in Table 1. The sample Al20Ca20Mg60 (at.% is generally used) was sealed in silica tubes and annealed at

300 °C for 3 weeks. All other samples (as-cast, from arc melting, rapidly cooled) were powdered in a steel ball mill for investigation by XRD to determine the phases present. The measurements were performed using a Siemens D5000 diffractometer with steps of 0.02° the diffraction angle range 2Θ and 3 s exposition time in the point. The obtained diffraction patterns were analyzed quantitatively using the program PowderCell 2.1 [1999Pow].

Thermal analysis was performed on four alloys with the compositions Al15Ca70Mg15, Al20Ca20Mg60, Al36.67Ca33.33Mg30 and Al45Ca40Mg15 using a Netzsch DTA 404 apparatus. The pre-molten sample was sealed under argon by welding in a tantalum crucible to avoid evaporation and oxidation. The DTA measurements were carried out under vacuum with heating/cooling rates of 5 and 1 K/min. Each sample was heated and cooled several times for the precise determination of peak positions and to ensure reproducibility of data. The estimated error of measurements is ±5 K. Difference between heating and cooling peaks was in most cases lower than 4 K. Some thermal effects showed large undercooling. After the DTA measurements all samples was investigated again by XRD.

The microstructures of the alloys after quenching and after the thermoanalytical measurements were examined by optical and scanning electron microscopy. The samples were ground and polished under alcohol to avoid reaction with water. Etching was not necessary since the alcohol already etched the surface of the polished samples. Ca-rich alloys reacted fast with oxygen and showed immediately corroded surfaces in air. This corrosion intensified the contrast between the grains in the microstructure.

4. Experimental results

Table 1 shows the compositions and the phase content derived from XRD, metallographic and SEM/EDX/WDX analyses of all investigated samples. The primary cristallizing phases are indicated in bold. For the alloys near the liquidus edge $CaMg_2$+Al_2Ca rod-like crystals with varying composition are observed. This phenomenon will be discussed later. The largely scattering EDX data were only used for qualitative phase identification.

Crystallographic data of the solid phases occurring inside the ternary Al−Ca−Mg system are given in Table 2. The maxium solubilities measured by XRD and SEM/EDX/WDX are also given in Table 1. Three binary phases dissolve remarkable contents of the third element: $CaMg_2$ up to 22 at.% Al, Al_2Ca up to 5 at.% Mg and Al_3Ca_8 up to 10 at.% Mg.

The phase compositions of three alloys were measured quantitatively by SEM/WDX.

The maximum solubilities of $CaMg_2$ (23 at.% Al) and Al_2Ca (6 at.% Mg) were determined by the alloys Al20Ca20Mg60 and Al45Ca40Mg15 using SEM/WDX and also by X-ray methods using Vegards's law. The composition of the residual liquid at the invariant reaction E_1/ U_2 was found to be around 29 at.% Al, 13 at.% Mg and 58 at.% Ca from alloy Al45Ca40Mg15. The approximate compositions of U_1 and Max_1 were estimated by this method, too. The results of the thermoanalytical analyses are given in Table 3. Their interpretation will discussed in conjunction with the results of the thermodynamic calculation.

It is remarkable that the ternary solid solubilities do not vary substantially with temperature. This is confirmed not only from the comparison of the as-cast versus heated at 300 °C/ 3 weeks alloy but also from XRD analysis of lattice parameter variations in as-cast versus DTA-treated alloys.

5.Thermodynamic calculation of phase diagrams

5.1. Binary subsystems

For a preliminary calculation data sets from published binary assessments were taken for all three subsystems. The Al−Ca system was investigated by [1994Ang]. The Al−Mg system was recently optimized by [1998Lia] and the Ca−Mg system by [1995Aga]. These data were used for a first extrapolation of the ternary system and to plan sample compositions for the investigation of the ternary system. After finishing the new data set for binary the Al−Ca phase diagram including the new phases AlCa and Al_3Ca_8 [2001Kev2], this data set was used for all further calculations. The program Pandat [2000Pan, 2001Che] was used for all calculations in this work.

The Gibbs energy function $G_i^{0,\phi}(T) = G_i^{\phi}(T) - H_i^{\mathrm{SER}}$ for the element *i* (*i*=Al, Ca, Mg) in the ϕ phase (ϕ = face-centered cubic [fcc] (Al, αCa), body-centered cubic [bcc] (βCa) and hexagonal-closed packed [hcp] (Mg), or liquid) is described by the equation:

$$G_i^{0,\phi}(T) = a + b \cdot T + c \cdot T \cdot \ln T + d \cdot T^2 + e \cdot T^3 + f \cdot T^{-1} + g \cdot T^7 + h \cdot T^{-9} \qquad (1)$$

where H_i^{SER} is the molar enthalpy of the stable element reference (SER) at 298.15 K and 1 bar, and *T* is the absolute temperature. The Gibbs energy functions for Al, Ca and Mg are taken from the SGTE compilation by Dinsdale [1991Din].

5.2. Ternary modeling

The liquid, fcc (Al, αCa), bcc (βCa) and hcp (Mg) solution phases are described by the substitutional solution model. For the liquid phase (L) the molar Gibbs energy is expressed by following equation:

$$\begin{aligned} G^{\mathrm{Liq}} &= x_{\mathrm{Al}} G^{0,\mathrm{Liq}}_{\mathrm{Al}} + x_{\mathrm{Ca}} G^{0,\mathrm{Liq}}_{\mathrm{Ca}} + x_{\mathrm{Mg}} G^{0,\mathrm{Liq}}_{\mathrm{Mg}} \\ &\quad + RT\left(x_{\mathrm{Al}} \ln x_{\mathrm{Al}} + x_{\mathrm{Ca}} \ln x_{\mathrm{Ca}} + x_{\mathrm{Mg}} \ln x_{\mathrm{Mg}}\right) + x_{\mathrm{Al}} x_{\mathrm{Ca}} x_{\mathrm{Mg}} \cdot L^{0} \end{aligned} \tag{2}$$

in which R is the gas constant, and x_{Al}, x_{Ca} and x_{Mg} are the molar fractions of Al, Ca and Mg. The interaction parameter L^0 may be linearly temperature dependent and is optimized for the liquid phase.

The three phases $CaMg_2$, Al_2Ca and Al_3Ca_8 were modelled as line-compounds $Ca_1(Mg,Al)_2$, $Ca_1(Al,Mg)_2$ and $Al_3(Ca,Mg)_8$ to reflect the experimentally observed ternary solubilities. The Gibbs energy (per mole of atoms) for $CaMg_2$ and Al_2Ca is expressed by

$$\begin{aligned} G^{\phi} &= y_{\mathrm{Al}}\, G^{0,\phi}_{\mathrm{Ca:Al}} + y_{\mathrm{Mg}}\, G^{0,\phi}_{\mathrm{Ca:Mg}} + \frac{2}{3} RT\left(y_{\mathrm{Al}} \cdot \ln y_{\mathrm{Al}} + y_{\mathrm{Mg}} \cdot \ln y_{\mathrm{Mg}}\right) \\ &\quad + y_{\mathrm{Al}} \cdot y_{\mathrm{Mg}} \cdot L^{0,\phi}_{\mathrm{Ca:Al,Mg}} \end{aligned} \tag{3}$$

in which y_{Al} and y_{Mg} are the site fractions of Al and Mg on the second sublattice. Similary, for Al_3Ca_8 we have

$$\begin{aligned} G^{\mathrm{Al3Ca8}} &= y_{\mathrm{Ca}}\, G^{0,\phi}_{\mathrm{Al:Ca}} + y_{\mathrm{Mg}}\, G^{0,\phi}_{\mathrm{Al:Mg}} + \frac{8}{11} RT\left(y_{\mathrm{Ca}} \cdot \ln y_{\mathrm{Ca}} + y_{\mathrm{Mg}} \cdot \ln y_{\mathrm{Mg}}\right) \\ &\quad + y_{\mathrm{Ca}} \cdot y_{\mathrm{Mg}} \cdot L^{0,\phi}_{\mathrm{Al:Ca,Mg}} \end{aligned} \tag{4}$$

The parameters $G^{0,\phi}_{i:j}$ (also called compound energies) are expressed relative to the Gibbs energies of the pure elements (Ca-fcc, Al-fcc, Mg-hcp) at the given temperature T. The proper compound energies $G^{0,\mathrm{CaMg2}}_{\mathrm{Ca:Mg}}$ and $G^{0,\mathrm{Al2Ca}}_{\mathrm{Ca:Al}}$ represent the stable binary $CaMg_2$ and Al_2Ca phases. The values are taken from the binary description of the Ca−Mg [1995Aga] and Al−Ca [2001Kev2] systems. The metastable terminal compounds $G^{0,\mathrm{CaMg2}}_{\mathrm{Ca:Al}}$ and $G^{0,\mathrm{Al2Ca}}_{\mathrm{Ca:Mg}}$ are given a positive value of 5 kJ/mol for the

Gibbs energy of formation. The L^0 parameter represents the interactions primarily within the sublattice. The $Al_3(Ca,Mg)_8$ phase is modelled in a similar way according to Eq. (4).

The parameters for the phases $CaMg_2$ and Al_2Ca were determined from the measured maximum solubilities and from the invariant reaction L = $CaMg_2$ + Al_2Ca (Max_1) which was measured at 735 °C. The calculated isothermal section of the Al−Ca−Mg system at 300 °C is given in Fig. 1. The investigated sample compositions are shown in different symbols according to the phase analysis. The arrows point to the measured phase compositions. A calculated vertical section from $CaMg_2$ to Al_2Ca is given in Fig. 2 including the DTA signals measured in this work. The experimental observation that the solid state equilibria and the ternary solubilities are largely temperature independent is most clearly reflected by the solvus lines in Fig. 2. The calculated liquidus surface is shown in Fig. 3. It is dominated by the highly stable phases $CaMg_2$ and Al_2Ca. The four alloys investigated by DTA are marked by open circles. Figures 4 and 5 show the calculated vertical section at constant 20 at.% Ca and 15 at.% Mg in comparison with the present DTA results. The calculated invariant reactions involving the liquid phase are shown in Table 4 compared to the present experimental data. The microstructures shown in Figs. 6 - 10 will be discussed below.

6. Discussion and conclusion

Published data for the ternary Al−Ca−Mg system concern only the Mg-rich corner. Based on these literature data alone, the phase diagram appears to be very simple with tie lines only from (Mg) to the stoichiometric phases $CaMg_2$, Al_2Ca and to γ ($Mg_{17}Al_{12}$). Preliminary extrapolation of the ternary system using the available data for the binary subsystems apparently confirmed this assumption. To check these phase relations given by the preliminary calculation, the first series of alloys was prepared. Since the observed microstructures of these alloys showed some discrepancies to the preliminary calculation, a second series with Ca-richer alloys was prepared. These alloys gave clear hints for additional binary Al−Ca phases. Therefore a detailed investigation of the binary Al-Ca system was performed. This resulted in a new Al−Ca phase diagram which we published recently [2001Kev1, 2001Kev2]. Using these new binary data some but not all inconsistencies could be solved. Especially the alloys between the two phases $CaMg_2$ and Al_2Ca show strange rod-like primary crystallizing phases with variable compositions. Figure 6 illustrates the microstructure of six alloys near the liquidus edge L+$CaMg_2$+Al_2Ca, which appear to be quite similar to each other. These data could be easily misinterpreted as a primary crystallizing (rod-like) ternary phase with

large homogeneity range. But X-ray analysis shows no hint for an additional phase. It should be mentioned that the identification of the binary phases $CaMg_2$, Al_2Ca and Al_3Ca_8 by X-ray diffraction is complicated by their large solubilities and the resulting large variations of their lattice parameters. So the last series of ten alloys was prepared along the quasibinary section $CaMg_2$-Al_2Ca to investigate the ternary solubility and lattice parameters of $CaMg_2$ and Al_2Ca. Only the combination of all results, X-ray, microstructure, SEM/EDX/WDX and DTA, leads to the conclusion that these remarkable rod-like crystals are an intergrowth between $CaMg_2$ and Al_2Ca. They are formed essentially during the monovariant eutectic reaction $L \rightarrow CaMg_2 + Al_2Ca$ and cannot be distinguished from the small amount of primary phase. This intergrowth is so dearly that it is difficult to be revealed by microscopy.

Alloys remote from this eutectic trough show normal microstructure. Figure 7 shows an optical microscopic image of sample Al20Ca60Mg20 with $CaMg_2$ as large primary crystals and some amount of eutectic containing the additional phases Al_3Ca_8 and (Ca). This solidification path may be calculated using the thermodynamic data but may also be estimated from Fig. 6. The microstructure of alloy Al16.67Ca33.33Mg50 given in Fig. 8 consists almost solely of phase $CaMg_2$. This is most reasonable in view of the phase diagrams in Figs. 6 and 2 and clearly demonstrates that the rapid quenching of this arc-melted sample results in solidification near equilibrium.

A different microstructure is observed if the primary phase is Al_2Ca as for alloy Al46.67Ca33.33Mg20 in Fig. 9. The relatively long path of single-phase Al_2Ca precipitation (see Fig. 6) results in a large, coherent and not rod-like Al_2Ca matrix with some amount of entrapped eutectic according to the nonvariant reaction Max_1, $L=CaMg_2+Al_2Ca$. The optical microscopic image of sample Al30Ca60Mg10 in Fig. 10 gives again a different microstructure. This alloy composition, just at the edge of the Al_2Ca-primary field (see Fig. 6), is near the composition of the transition type reaction U_2 and the ternary eutectic E_1. It consists of the phases Al_3Ca_8, $CaMg_2$ with small amounts of Al_2Ca. This is in reasonable agreement with the calculated phase equilibria.

In the subsolidus region the calculated phase relations are in good agreement with all experimental data as given essentially in Fig. 1. For the tie triangle (Ca) + Al_3Ca_8 + $CaMg_2$ the calculated compositions of Al_3Ca_8 and $CaMg_2$ are not far from their maximum solubilities at 300 °C. However the EDX data in Table 1 give smaller values for that triangle, around 2 at.% Mg for Al_3Ca_8 and 4 at.% Al for $CaMg_2$, which is attributed to the only qualitative nature of that measurement. The more important maximum solubilities are based on the WDX and XRD data in good agreement with the calculation.

Only the first order interaction parameters are used to model the ternary solubilities. The linear temperature dependence of these interaction parameters L^0 is determined from the measured temperatures of the maximum Max_1: L = Al_2Ca + $CaMg_2$ at 735 °C (calculated at 738 °C) and the reaction E_2: L = βCa + $CaMg_2$ + Al_3Ca_8 at 410 °C (calculated at 444 °C). The maxmium of the liquidus of $CaMg_2$ (Fig. 2) is real and related to the large solid solubility. These high liquidus temperatures of $CaMg_2$ are measured in fact by DTA in the alloy Al20Ca20Mg60 (Fig. 4) and Al15Ca70Mg15 (Fig. 5). The calculated invariant reactions U_1, U_2 and E_2 are confirmed satisfactorly by DTA and SEM/WDX results. Because of their internal consistency with smooth thermodynamic functions, the calculated results are preferred to individual experimental data.

This study was supported by the German Research Council (DFG) under Grant No. Schm 588/25-1.

References

[1948Por] Portnoi, K.I., Spektorova, S.I.: Express Information, Intsagi, B, 19 (1948) 5.
[1957Cat] Catterall, J.A., Pleasance, R.J.: J. Inst. Met. 86 (1957-58) 189.
[1958Sta] Stacey, R.D.: U.K. Atomic Energy Authority, Industrial Group Report, R & DB(S) TN-2167 (1958).
[1959Dow] Dow Chemical Co. Midland, MI, Dow Chemical Co. Report 15004, U.S. Govt. Res. Reports, 31 (1959) 355.
[1981Mak] Makhmudov, M.M., Vakhobov, A.V., Dzhuraev, T.D.: Russ. Metall., (6) (1981) 209.
[1985Vil] Villars, P., Calvert, L.D.: Pearson's Handbook of Crystallographic Data for Intermetallic Phases, ASM, Metals Park, Ohio (1985).
[1991Din] A.T. Dinsdale: CALPHAD 15 (1991) 317.
[1994Ang] Anglezio, C., Ansara, I.: CALPHAD 18(3) (1994) 273.
[1995Aga] Agarwal, R., Lee, J. J., Lukas, H.-L., Sommer, F.: Z. Metallkd. 86 (1995) 103.
[1998Lia] Liang, P., Su, H.-L., Donnadieu, P., Harmelin, M.G., Quivy, A., Ochin, P., Effenberg, G., Seifert, H.J., Lukas, H.L., Aldinger, F.: Z. Metallkd. 89(8) (1998) 536.
[1999Pow] PowderCell for Windows, Version 2.3 (1999), W. Kraus & G. Nolze, Federal Institute for Materials Research and Testing, Berlin.
[2000Luo] Lou, A.A., in: Kaplan, H.I., Hryn, J., Clow, B.B. (Eds.): Magnesium Technology 2000, TMS, Warrendale, PA (2000) 89.
[2000Pan] Pandat - Phase Diagram Calculation Engine for Multicomponent Systems, CompuTherm LLC, 437 S. Yellowstone Dr., Suite 217, Madison, WI (2000).
[2001Che] Chen, S.-L., Daniel, S., Zhang, F., Chang, Y.A., Oates, W.A., Schmid−Fetzer, R.: J. Phase Equilibria 22 (2001) 373.
[2001Kev1] Kevorkov, D., Schmid−Fetzer, R.: Z. Metallkd. 92 (2001) 946.
[2001Kev2] Kevorkov, D., Schmid−Fetzer, R., Pisch, A., Hodaj, F., Colinet, C.: Z. Metallkd. 92 (2001) 953.
[2001Luo] Lou, A.A., Powell, B.R., in: Kaplan, H.I. (Ed.), Magnesium Technology 2001, TMS,

Warrendale, PA (2001) 137.
[2001Pek] Pekguleryuz, M.O., Baril E.: Mat. Trans. 42 (2001) 1258.
[2001Wan] Wang Q.D., Chen W.D., Zeng X.Q., Lu Y.Z., Ding W.J., Zhu Y.P., Xu X.P., Mabuchi M.: J. Mater. Science 36 (2001) 3035.
[2001You] You B.S., Park W.W., Chung I.S.: Mater. Trans. 42 (2001) 1139.
[2002Buc] F. v. Buch, S. Schumann, H. Friedrich, E. Aghion, B. Bronfin: Metall 56 (2002) 40.

Correspondence address:

Prof. Dr. R. Schmid-Fetzer

Technical University of Clausthal, Institute of Metallurgy

Robert-Koch-Str. 42

D-38678 Clausthal-Zellerfeld, Germany

Tel.: +49-5323-72 2150

Fax: +49-5323-72 3120

E-mail: schmid-fetzer@tu-clausthal.de

Table 1 Composition and phase content of samples investigated at room temperature. Phase identification by XRD, metallography and SEM/EDX, partly SEM/WDX.

Sample composition (at.%)	Identified phases and solubilities (at.%) (primary solidified phase in bold)
Al15Ca70Mg15	**$CaMg_2$** (EDX: 4 % Al) + Al_3Ca_8 (EDX: 2 % Mg)+ (Ca)
Al20Ca70Mg10	**$CaMg_2$** (EDX: 4 % Al) + Al_3Ca_8 + (Ca)
Al20Ca60Mg20	**$CaMg_2$** (EDX: 4 % Al) + Al_3Ca_8 + (Ca)
Al30Ca60Mg10	$CaMg_2$ + Al_3Ca_8 + Al_2Ca
Al25Ca50Mg25	**$CaMg_2$** (EDX: 14 % Al) + Al_3Ca_8 (EDX: 6 % Mg) + Al_2Ca*
Al30Ca50Mg20	**$CaMg_2$** (EDX: 14 % Al) + Al_3Ca_8 (EDX: 7 % Mg) + Al_2Ca*
Al35Ca50Mg15	$CaMg_2$ (EDX: 8 % Al) + Al_3Ca_8 (EDX: 7 % Mg) + **Al_2Ca***
Al34Ca46Mg20	$CaMg_2$ (EDX: 9 % Al) + Al_3Ca_8 (EDX: 7 % Mg) + **Al_2Ca***
Al30Ca45Mg25	$CaMg_2$ + Al_3Ca_8 + **Al_2Ca***
Al40Ca40Mg20	$CaMg_2$ (EDX: 15 % Al) + Al_3Ca_8 (EDX: 7 % Mg) + **Al_2Ca***
Al45Ca40Mg15	Al_3Ca_8 + Al_2Ca (WDX: 6 % Al)*
Ca33.33Mg66.67	**$CaMg_2$**
Al6.67Ca33.33Mg60	**$CaMg_2$**
Al16.67Ca33.33Mg50	**$CaMg_2$**
Al26.67Ca33.33Mg40	$CaMg_2$ + **Al_2Ca***
Al33.33Ca33.33Mg33.33	$CaMg_2$ + **Al_2Ca***
Al36.67Ca33.33Mg30	$CaMg_2$ + **Al_2Ca***
Al46.67Ca33.33Mg20	$CaMg_2$ + **Al_2Ca***
Al50Ca33.33Mg16,67	$CaMg_2$ + **Al_2Ca** (EDX: 6 % Mg)
Al56.67Ca33.33Mg10	$CaMg_2$ + **Al_2Ca** (EDX: 4 % Mg)
Al66.67Ca33.33	**Al_2Ca**
Al36Ca28Mg36	**Al_2Ca*** + $CaMg_2$ (EDX: 3 % Al) + (Mg)
Al43Ca27Mg30	**Al_2Ca*** + $CaMg_2$ (EDX: 14 % Al) + (Mg)
Al30Ca25Mg45	**Al_2Ca*** + $CaMg_2$ (EDX: 15 % Al) + (Mg)
Al20Ca20Mg60**	Al_2Ca* + **$CaMg_2$** (EDX: 14 % Al, WDX: 23 % Al) + (Mg)

* Rod-like crystals which were recognized as intergrowth of the phases Al_2Ca and $CaMg_2$ were formed in the appearance of primary phase.

** Constitution does not change after annealing for three weeks at 300 °C

Table 2 Solid phases extending into the in the ternary Al–Ca–Mg system.

Phase Temperature	Pearson symbol Prototype	Lattice parameters (pm)	Phase composition	Ref.
Al_2Ca < 1086 °C	cF24 $MgCu_2$	a=803.8 a=807.6	at 0 at.% Mg at 5 at.% Mg $(Al,Mg)_2Ca$	[1985Vil] This work
Al_3Ca_8 < 579 °C	aP22 Ca_8In_3	a=949.50, α=99.057° b=959.22, β=101.152° c=967.04, γ=119.613° a=926.0, α=99.48° b=946.6, β=99.42° c=978.0, γ=119.89°	at 0 at.% Mg at 10 at.% Mg $Al_3(Ca,Mg)_8$	[2001Kev1] This work
$CaMg_2$ < 715 °C	hP12 $MgZn_2$	a=623 c=1015 a=607 c=973	at 0 at.% Al at 22 at.% Al $Ca(Mg,Al)_2$	[1985Vil] This work

Table 3 Results of the thermoanalytic analysis and their interpretation

Sample composition (at.%)	Heating/ cooling rate (K/min)	DTA signals[a)] (°C)	Assessed experimental temp. [b)] (°C)	Phase boundary or invariant reaction, calculated temperature (°C)
Al15Ca70Mg15	1	491 c	491 liq	486: L / L + $CaMg_2$
	1	495 h		
	1	409 c	410 inv	444 E_2: L = βCa + $CaMg_2$ + Al_3Ca_8
	1	413 h		
Al20Ca20Mg60	1	718 c	718 liq	718: L / L + $CaMg_2$
	5	625 h	620 weak	552: L + $CaMg_2$ / L + $CaMg_2$ + Al_2Ca
	5	627 c		
	5	514 h/ 511 c	511 inv	512 U_1: L + $CaMg_2$ = Al_2Ca + (Mg)
	1	514 h/ 511 c		
Al36.67Ca33.33 Mg30	1	826 h/ 809 c	810 liq	797: L / L + Al_2Ca
	1	736 h/ 734 c	735 inv	738 Max_1: L = Al_2Ca + $CaMg_2$
	1	484 c	484 weak	484 U_2[c)]:L + Al_2Ca = $CaMg_2$ + AlCa
Al45Ca40Mg15	1	935 h/ 934 c	934 liq	872: L / L + Al_2Ca
	1	705 h	705 very weak	713: L + Al_2Ca / L + Al_2Ca + $CaMg_2$
	1	506 h	506	504 U_2: L + Al_2Ca = $CaMg_2$ + AlCa
	1	489 h/484 c	484 inv	
	1	458 h/ 452 c	455 weak	? 444 Max_4: L = βCa + $CaMg_2$ + Al_3Ca_8
	1	410 h/ 409 c	409 inv	?

a) c = cooling (onset), h = heating (onset for invariant reactions, peak maximum otherwise).
b) inv = large and sharp signal with no significant undercooling, liq = liquidus.
c) for Ca-excess sample.

Table 4 Invariant reactions with liquid (L) in the ternary system Al–Ca–Mg

Invariant reaction		Experimental				Calculated; this work		
	Type	T [°C]	x_{Al}^{Liquid}	x_{Mg}^{Liquid}	Ref.	T [°C]	x_{Al}^{Liquid}	x_{Mg}^{Liquid}
$L = Al_2Ca + CaMg_2$	Max_1	735	0.41	0.23	This work	738	0.367	0.30
$L = Al_2Ca + (Mg)$	Max_2	535	–	0.78–79	[59Dow]	[a]		
$L + CaMg_2 = Al_2Ca + (Mg)$	U_1	?	0.09	0.79	[48Por]	–	–	–
	U_1	511	0.12	0.80	This work	512	0.19	0.75
$L + Al_2Ca = CaMg_2 + AlCa$	U_2	484	0.29	0.13	This work	504	0.29	0.09
$L = Al_3Ca_8 + CaMg_2$	Max_3					492	0.26	0.10
$L = Al_3Ca_8 + AlCa + CaMg_2$	E_1					488	0.28	0.08
$L = \beta Ca + CaMg_2 + Al_3Ca_8$	E_2	410	0.13	0.19	This work	444	0.14	0.13
$L = Al_2Ca + \gamma$	Max_4					444	0.48	0.49
$L = Al_2Ca + Al_4Ca + \gamma$	E_3					443	0.51	0.46
$L = Al_4Ca + \beta + (Al)$	E_4					442	0.64	0.34
$L = Al_4Ca + \beta + \gamma$	E_5					438	0.58	0.40
$L = Al_2Ca + \gamma + (Mg)$	E_6					422	0.33	0.65

[a] No pseudobinary section –degenerated into U_2

Figures:

Fig. 1 Calculated isothermal section at 300 °C including our own results. Dots represent the investigated sample compositions, arrows point to the identified phases.
Three-phase triangles are shaded.

Fig. 2 Calculated vertical section $CaMg_2$ – Al_2Ca with DTA signals from alloy Al36.67Ca33.33Mg30. The weak signal at 484 °C may be due to a slight Ca excess of the sample and participation in the reaction U_2 (see Tables 3 and 4).

Fig. 3 Calculated liquidus surface including isotherms and four DTA sample compositions.

Fig. 4 Calculated vertical section at constant 20 at.% Ca with DTA signals from alloy Al20Ca20Mg60.

Fig. 5 Calculated vertical section at constant 15 at.% Mg with DTA signals from the alloys Al15Ca70Mg15 and Al45Ca40Mg15.

Fig. 6 Calculated liquidus surface with optical microscopic images of the microstructure of the alloys near the eutectic trough (solid circles). The four open circles indicate alloys with microstructures shown in Figs. 7 – 10. All alloys in as-cast condition.

Fig. 7 Optical microscopy image of sample Al20Ca60Mg20 (as-cast) showing the phase $CaMg_2$ (dark grey) as primary crystals.

Fig. 8 Optical microscopy image of sample Al16.67Ca33.33Mg50 (as-cast) showing a microstructure consisting almost entirely of phase $CaMg_2$.

Fig. 9 Optical microscopy image of sample Al46.67Ca33.33Mg20 (as-cast) showing the primary phase Al_2Ca.

Fig. 10 Optical microscopy image of sample Al30Ca60Mg10 (as-cast) showing a microstructure near U_2 consisting of the phases Al_3Ca_8, $CaMg_2$ and small amounts of Al_2Ca.

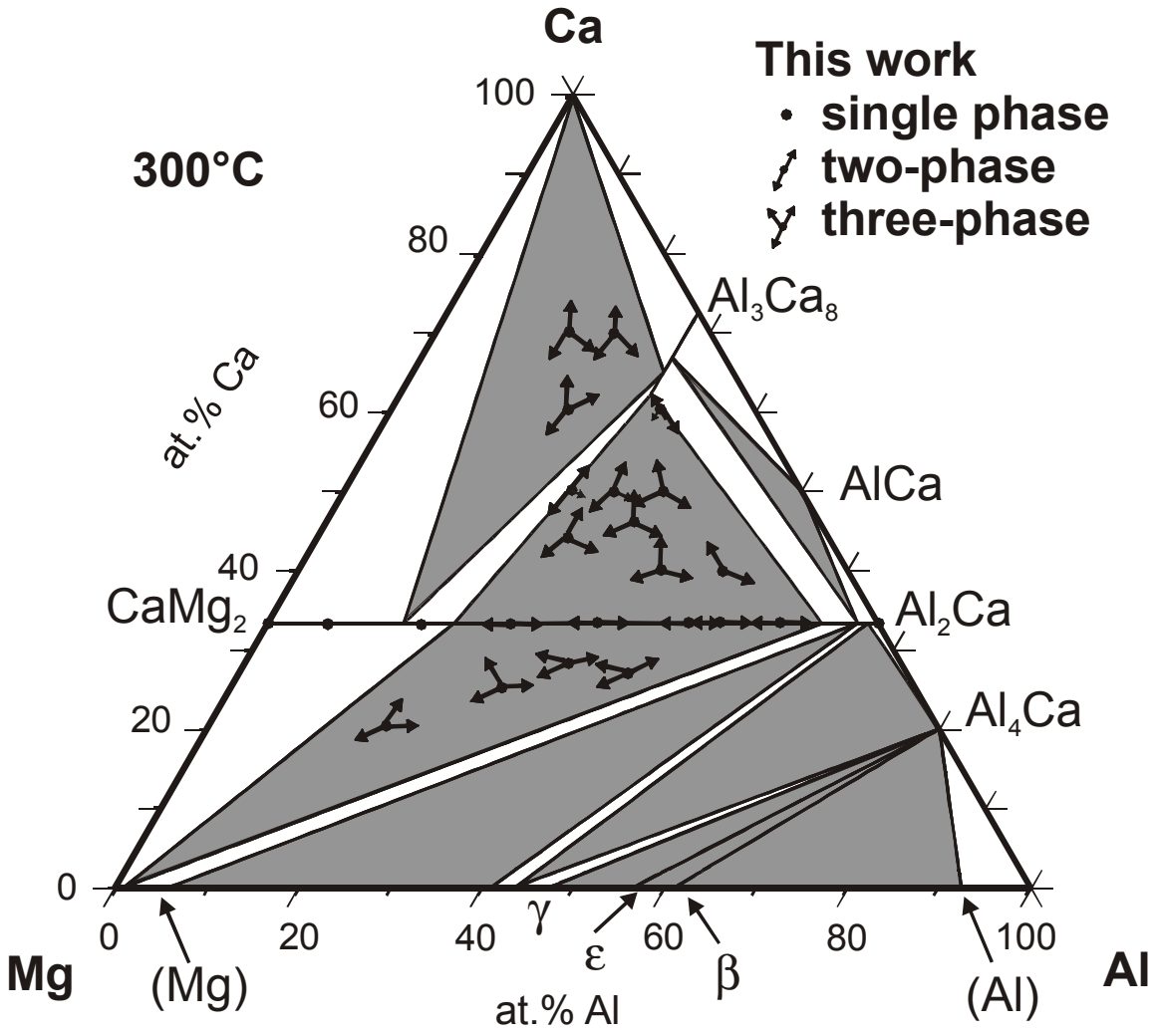

Fig. 1 Calculated isothermal section at 300 °C including our own results. Dots represent the investigated samples compositions, arrows point to the identified phases. Three-phase triangles are shaded.

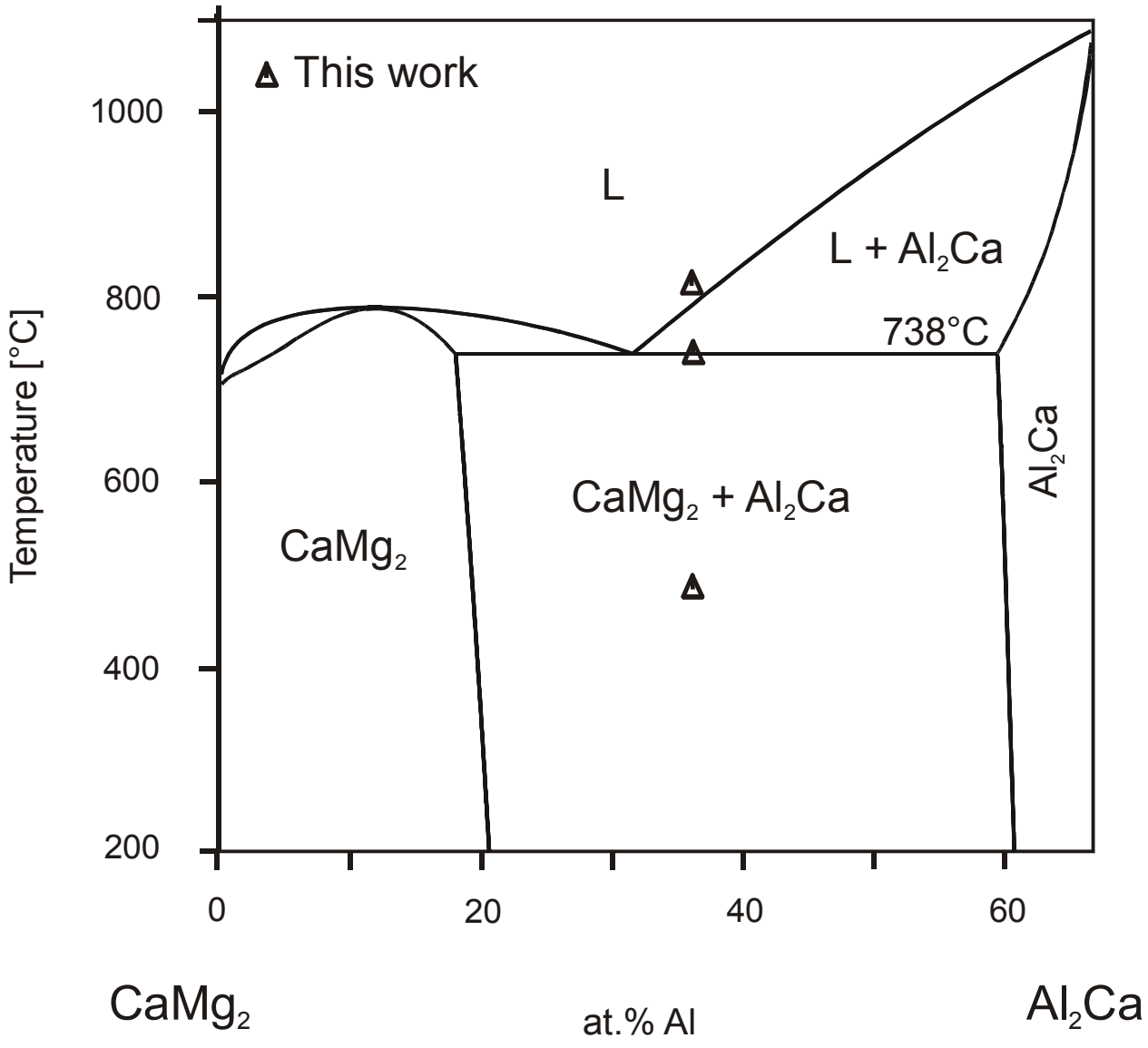

Fig. 2 Calculated vertical section $CaMg_2$ - Al_2Ca with DTA signals from alloy Al36.67Ca33.33Mg30. The weak signal at 484 °C may be due to a slight Ca excess of the sample and participation in the reaction U_2 (see Tables 3 and 4).

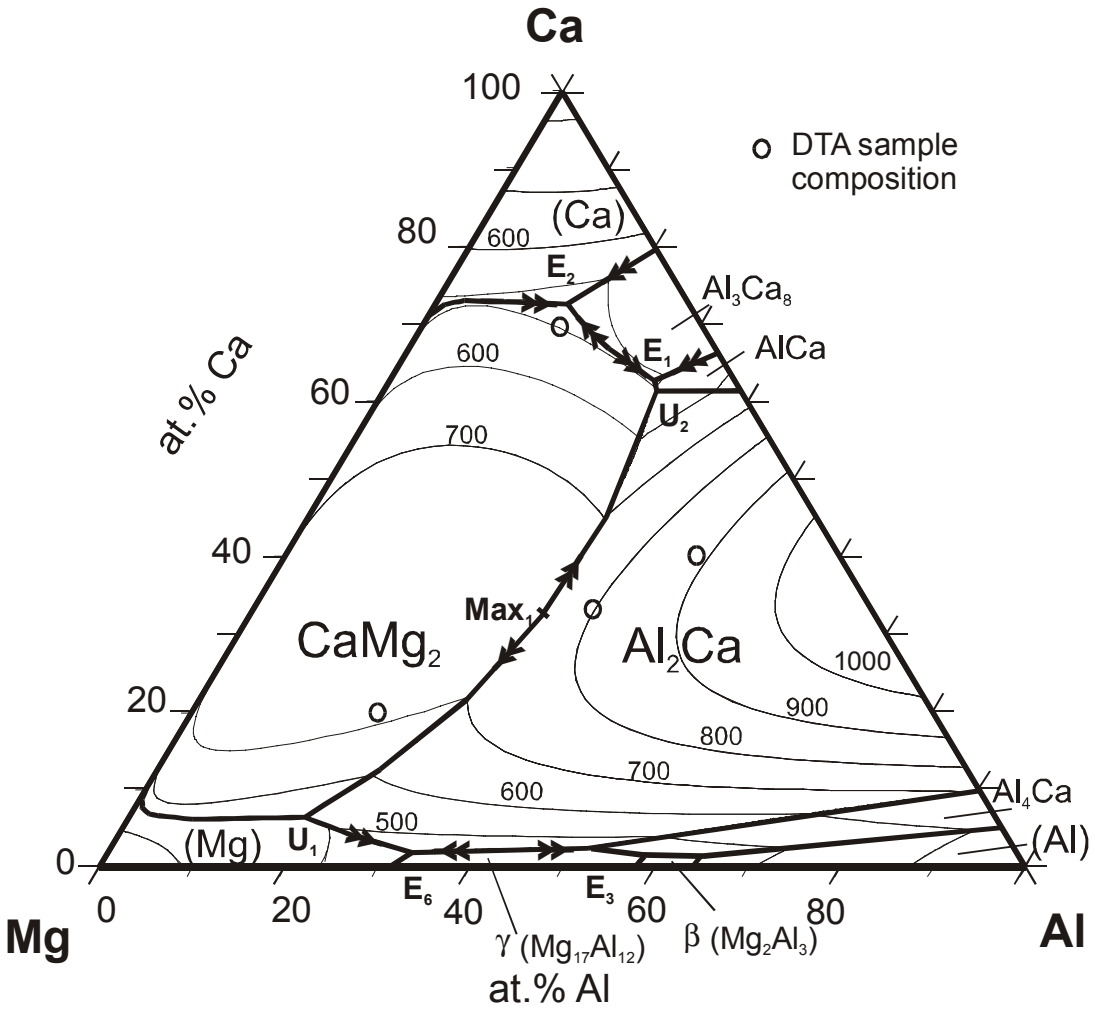

Fig. 3 Calculated liquidus surface including isotherms and four DTA sample compositions.

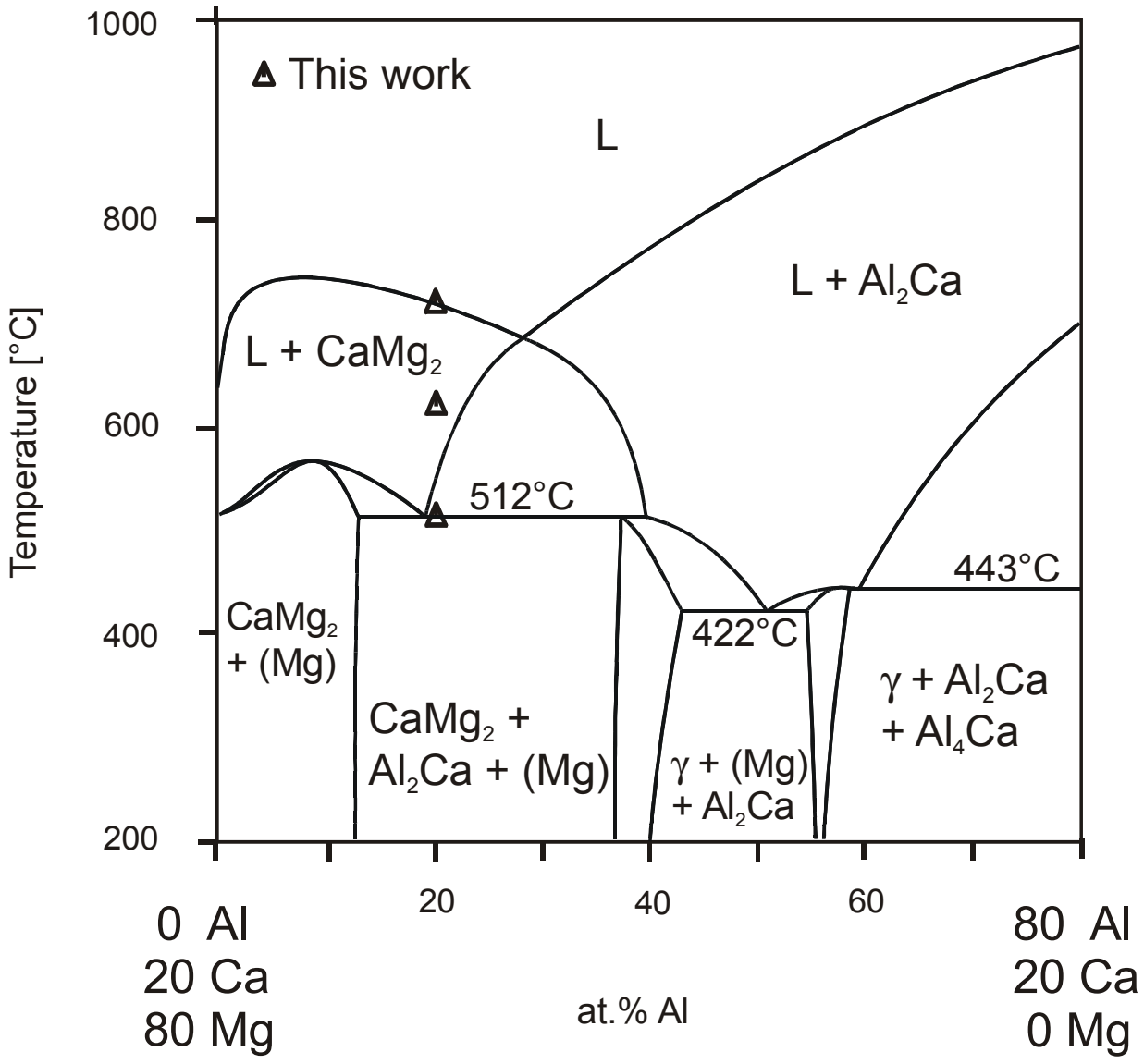

Fig. 4 Calculated vertical section at constant 20 at.% Ca with DTA signals from alloy Al20Ca20Mg60.

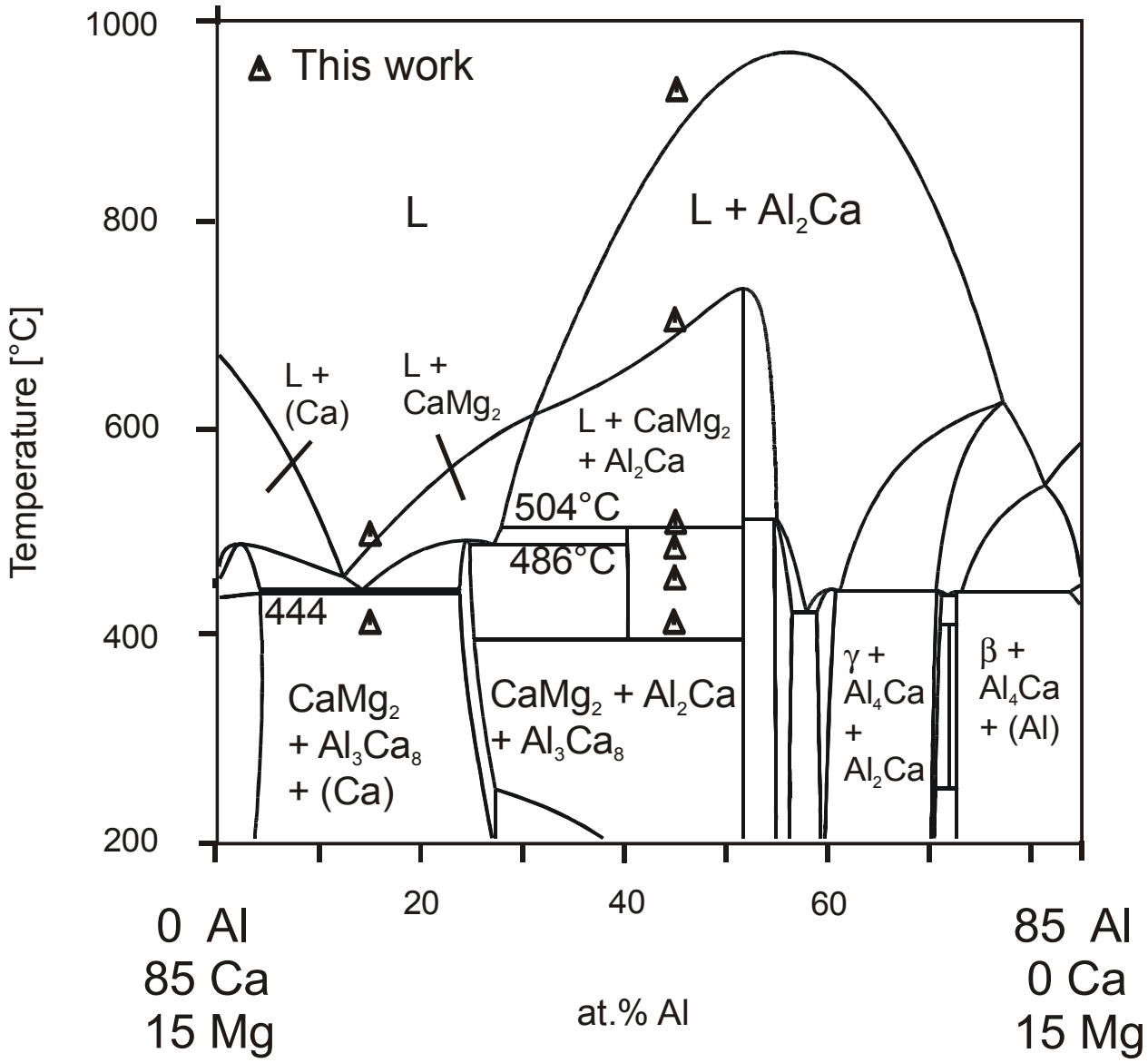

Fig. 5 Calculated vertical section at constant 15 at.% Mg with DTA signals from the alloys Al15Ca70Mg15 and Al45Ca40Mg15.

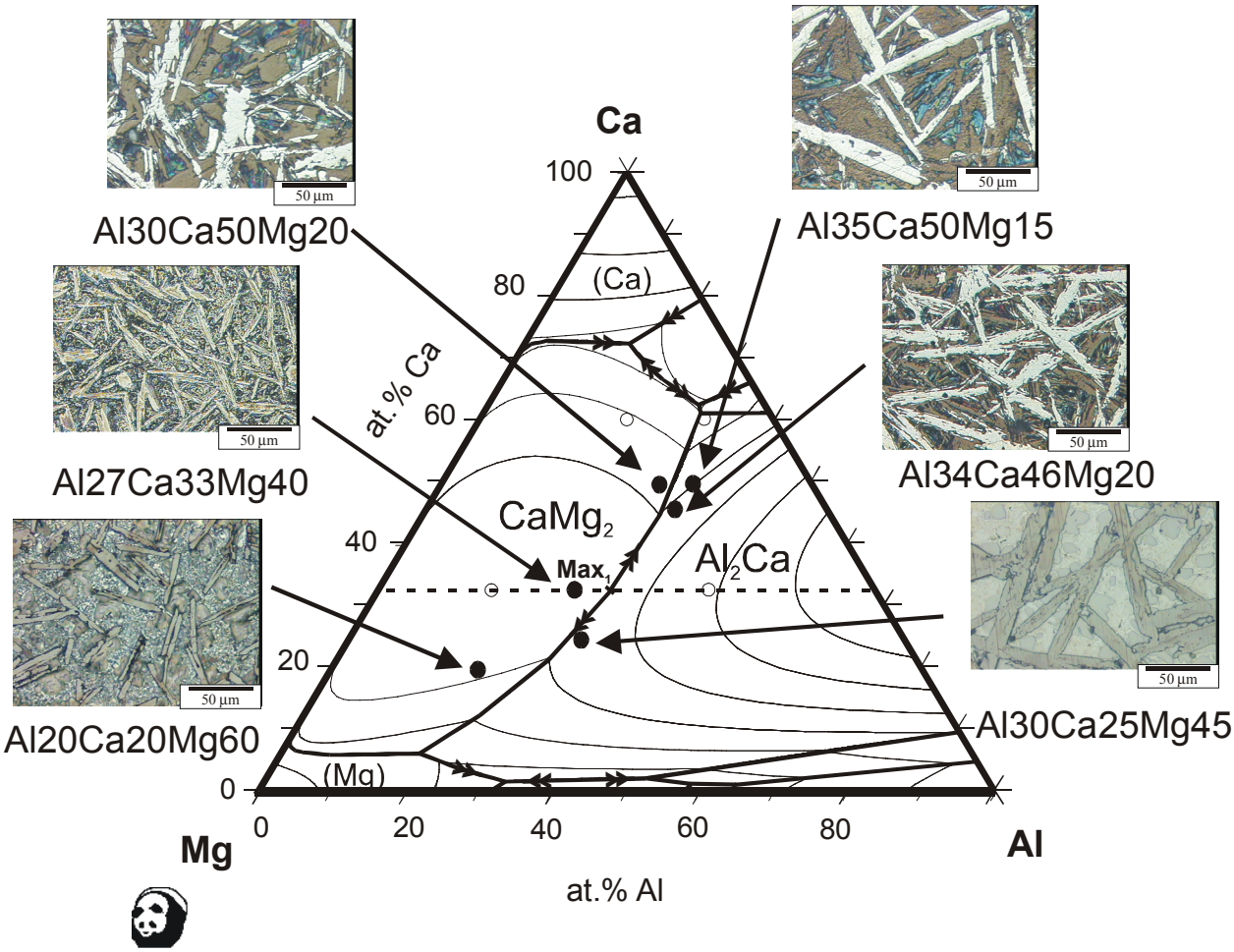

Fig. 6 Calculated liquidus surface with optical microscopic images of the microstructure of the alloys near the eutectic trough (solid circles). The four open circles indicate alloys with microstructures shown in Figs. 7 - 10. All alloys in as-cast condition.

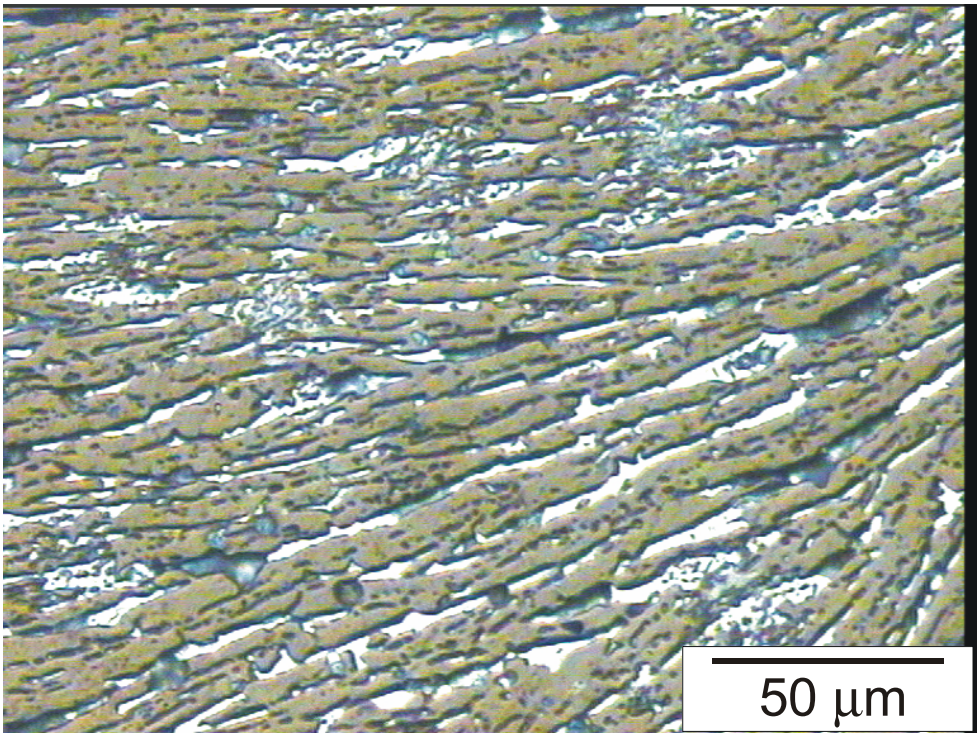

Fig. 7 Optical microscopy image of sample Al20Ca60Mg20 (as-cast) showing the phase $CaMg_2$ (dark grey) as primary crystals.

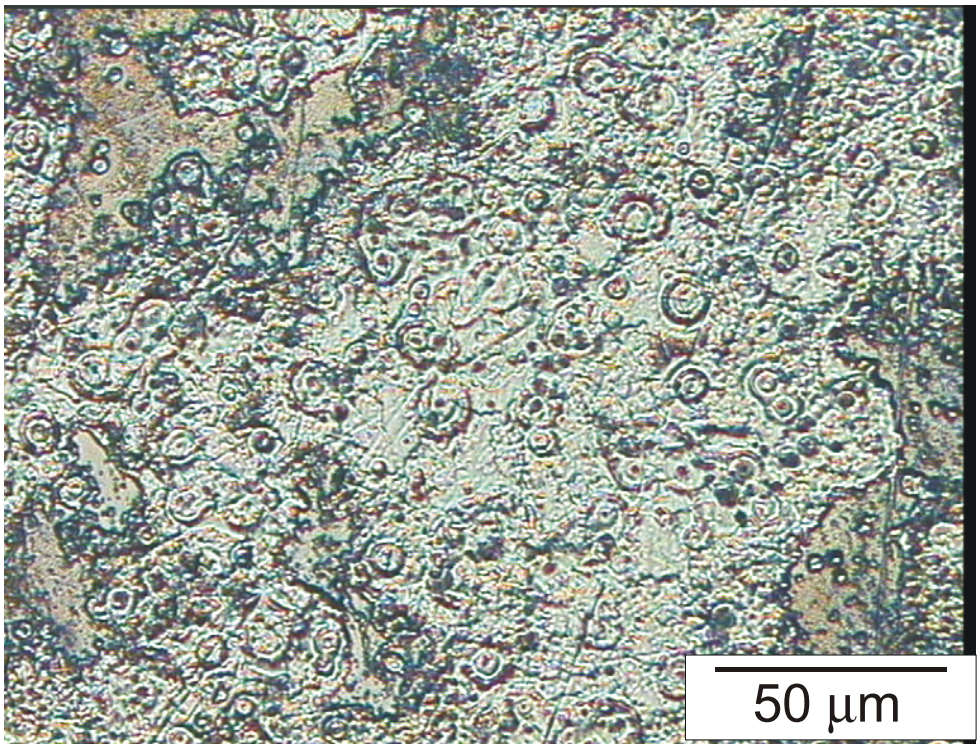

Fig. 8 Optical microscopy image of sample Al16.67Ca33.33Mg50 (as-cast) showing a microstructure consisting almost entirely of phase $CaMg_2$.

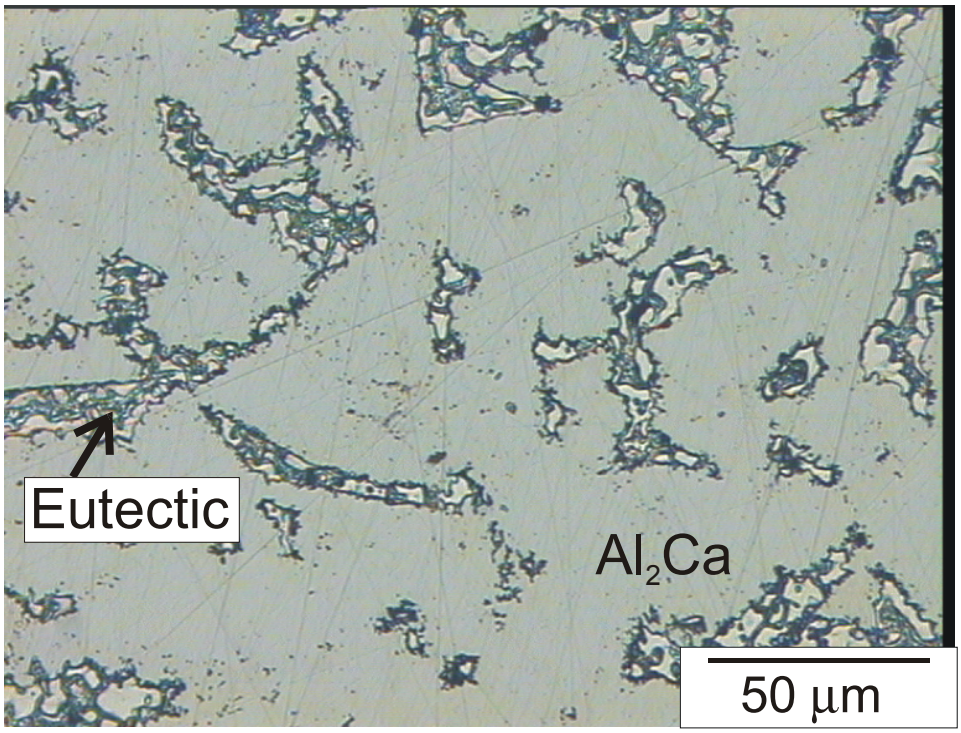

Fig. 9 Optical microscopy image of sample Al46.67Ca33.33Mg20 (as-cast) showing the primary phase Al_2Ca.

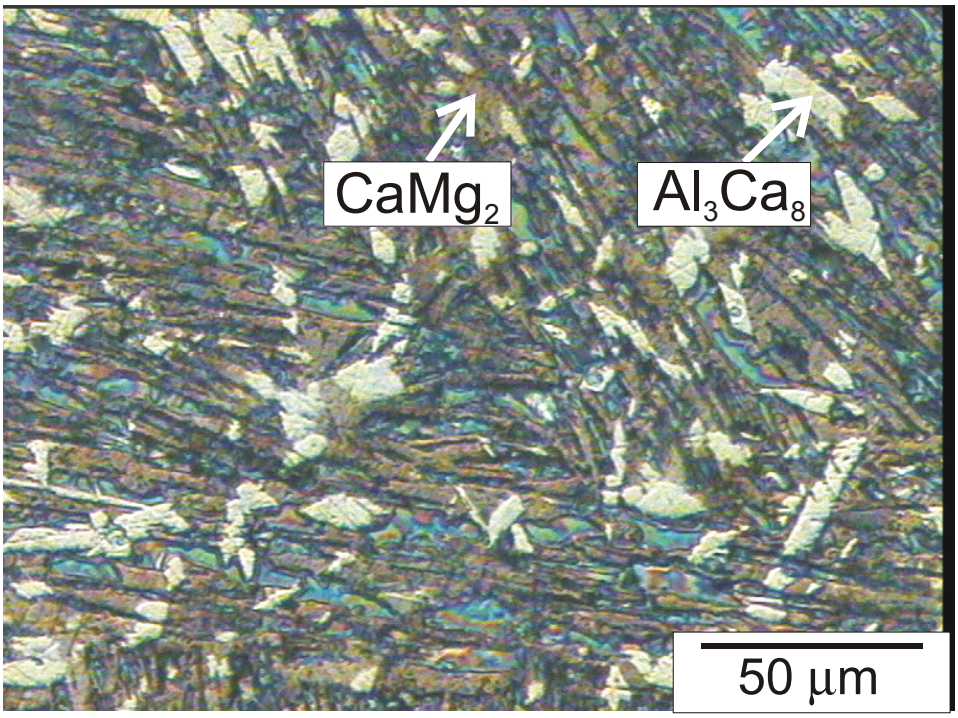

Fig. 10 Optical microscopy image of sample Al30Ca60Mg10 (as-cast) showing a microstructure near U_2 consisting of the phases Al_3Ca_8, $CaMg_2$ and small amounts of Al_2Ca.